Support Vector Regression for Improved Real-Time, Simultaneous Myoelectric Control

Ali Ameri, *Student Member, IEEE*, Ernest N. Kamavuako, *Member, IEEE*, Erik J. Scheme, *Member, IEEE*, Kevin B. Englehart, *Senior Member, IEEE*, and Philip A. Parker, *Life Senior Member, IEEE*

***Abstract*—This study describes the first application of a support vector machine (SVM) based scheme for real-time simultaneous and proportional myoelectric control of multiple degrees of freedom (DOFs). Three DOFs including wrist flexion–extension, abduction–adduction and forearm pronation–supination were investigated with 10 able-bodied subjects and two individuals with transradial limb deficiency (LD). A Fitts' law test involving real-time target acquisition tasks was conducted to compare the usability of the SVM-based control system to that of an artificial neural network (ANN) based method. Performance was assessed using the Fitts' law *throughput* value as well as additional metrics including *completion rate, path efficiency* and *overshoot.* The SVM-based approach outperformed the ANN-based system in every performance measure ($p < 0.05$) for able-bodied subjects. The SVM outperformed the ANN in *path efficiency* and *throughput* with the first LD subject and in *throughput* with the second LD subject. The superior performance of the SVM-based system appears to be due to its higher estimation accuracy of all DOFs during inactive and low amplitude segments (these periods were frequent during real-time control). Another advantage of the SVM-based method was that it substantially reduced the processing time for both training and real time control.**

***Index Terms*—Amputee, electromyogram (EMG), myoelectric control, simultaneous control, support vector machines.**

I. Introduction

THE ELECTROMYOGRAM (EMG) contains important neuromuscular information, and is widely used to control externally powered prostheses [1], robots [2], and human–computer interfaces (HCI) [3]. With this method, the motor intent is estimated from the EMG during muscle contractions [4]. Subsequently, the estimated intent becomes functional using an appropriate control scheme. For instance, with *velocity control*, the contraction intensity is proportional to the velocity of the device, while in *position control*, the intensity of effort is mapped to the device position or angular displacement.

A variety of approaches have been used to estimate motor intent. Current commercial prostheses use the EMG amplitude [5] or rate of change [6] measured from one or two muscles to control a degree-of-freedom (DOF) of an elbow, wrist or hand. However, more than one DOF at a time cannot be controlled with this approach. To change the DOF, a muscle co-contraction or hardware switch must be used [7], resulting in an unnatural multi-DOF control.

Extensive research has focused on pattern classification-based techniques [8]–[12] to accommodate control of more than one DOF. With these methods, the EMG patterns from multiple electrodes are classified into several classes of motion intent. However, most pattern classification based systems do not inherently provide proportional control. Recent work [13] showed that including proportional control reduced the classification accuracy unless the training protocol is changed. Furthermore, pattern classification-based systems typically do not allow simultaneous control, although preliminary work [14], [15] included simultaneous, but dependent motions (the outputs of different DOFs in combined motions are dependent as their intensities are always equal). Sequential control imposes cognitive burden upon the user and reduces the functionality.

To provide independent simultaneous control of DOFs, recent work has investigated the use of regression techniques to relate EMG to a continuous motor variable such as force or position. In the case of amputees, the force/position cannot be measured from the absent limb, and therefore a strategy termed *mirrored bilateral training* has been used in which the force/position is acquired from the opposite (intact) limb during *mirrored bilateral contractions* (e.g., [16]–[24]). This approach however, is limited to unilateral amputees.

To accommodate bilateral amputees, Jiang *et al.* [25] and Muceli *et al.* [26] proposed an unsupervised training approach for simultaneous control. Wrist flexion–extension and pronation–supination were investigated and the training involved single DOF contractions. For each trial, by applying non-negative matrix factorization to the EMG root mean square (rms) values, a non-negative synergy matrix was derived. The matrices from both DOFs were incorporated to form a complete synergy matrix, which was used in a real-time test for simultaneous control. Choi *et al.* [27] proposed a training method in which the users were prompted to produce contractions according to a target cursor on a computer display. Wrist flexion–extension and abduction–adduction were investigated

Manuscript received December 26, 2013; revised April 01, 2014; accepted May 09, 2014. Date of publication May 16, 2014; date of current version November 13, 2014. This work was supported by the Natural Sciences and Engineering Research Council of Canada (NSERC) under NSERC Discovery Grant 217354-10 and Grant A4445-2004.

A. Ameri, E. J. Scheme, K. B. Englehart, and P. A. Parker are with the Institute of Biomedical Engineering, and the Department of Electrical and Computer Engineering, University of New Brunswick, Fredericton, NB, E3B 5A3 Canada (e-mail: ali.ameri@unb.ca; escheme@unb.ca; kengleha@unb.ca; pap@unb.ca).

E. N. Kamavuako is with the Center for Sensory-Motor Interaction, Department of Health Science and Technology, Aalborg University, 9220 Aalborg, Denmark (e-mail: enk@hst.aau.dk).

Color versions of one or more of the figures in this paper are available online at http://ieeexplore.ieee.org.

Digital Object Identifier 10.1109/TNSRE.2014.2323576

and the training was performed using single DOF contractions. A non-negative synergy matrix was developed to map the EMG amplitudes to the cursor displacements. In a tracking test, the synergy matrix was used for EMG-based simultaneous control of a cursor.

In this work, a training protocol similar to that used in [27] was employed, but it involved both single and combined DOF contractions. For simultaneous estimation of DOFs, various linear and nonlinear estimators have been used in the literature, with multilayer perceptron ANNs as a common nonlinear approach (e.g., [16]–[22]). Kernel ridge regression (KRR) was employed in [23] for offline simultaneous estimation of wrist position in flexion–extension and abduction–adduction (transforming data to a higher dimensional space using a kernel trick is performed in both KRR and support vector regression). Support vector regression (SVR) has been previously used for single DOF, in offline force estimation for grasp [24], [28]–[30] (in [30] for different grasp types) and flexion–extension [31]. In this work, for the first time to our knowledge, *real-time simultaneous* myoelectric control is performed using SVR.

For usability evaluations in previous work, computer-based tests have been conducted which prompt a user to control a cursor or virtual limb to reach a target position or perform a particular task. Target achievement tasks have been widely assessed using Fitts' law [32] in HCI studies. Fitts' law is a model of human movement based on Shannon's work [33] in information theory. This describes a speed-accuracy trade-off in rapid pointing tasks and formulates the average time to reach a target as a function of target distance and size. It also provides a single performance metric in the form of throughput (in bits per second). Recent studies have employed Fitts' law to assess myoelectric control in virtual target reaching tasks (e.g., [34]–[37], [38]). These studies also utilize other performance measures in addition to throughput, to provide a more detailed evaluation.

In this paper, a 3-D Fitts' law test is conducted to compare the control quality of an SVM-based system to that of a baseline ANN-based scheme using various performance metrics.

II. Support Vector Regression

SVMs, first introduced by Vapnik *et al.* [39], [40], are supervised learning algorithms that can be used for both classification and regression. Assuming a set of training data, $\{(\boldsymbol{x_1}, y_1), \ldots, (\boldsymbol{x_n}, y_n)\}$, where each $\boldsymbol{x_i} \in R^N$, and $y_i \in R$, and n is the number of training examples, the goal is to find a regression function $f(\boldsymbol{x})$ that has at most a deviation of ε from the target (y) for all training data. Since choosing appropriate ε may be difficult, v-SVM was proposed in 1999 [41] for both classification and regression. With this method, an intuitive tunable parameter $0 < v < 1$ is employed which gives a lower bound on the fraction of support vectors and an upper bound on the fraction of margin errors. For support vector regression, the input data $(\boldsymbol{x})$ are mapped to a higher dimensional space by performing a nonlinear projection, in order to linearly estimate the regression function $f(\boldsymbol{x})$ from

$$f(\boldsymbol{x}) = \boldsymbol{w^T}\Phi(\boldsymbol{x}) + b \tag{1}$$

(a)

(b)

Fig. 1. Picture of the residual limb is shown for (a) LD subject I and (b) LD subject II.

where $\boldsymbol{\Phi(x)}$ is the nonlinear projection of the input data to the high dimensional feature space. SVR seeks the flattest function in the high dimensional space, or equivalently a small $\boldsymbol{w}$ in (1), which is ensured by minimizing the norm, i.e., $\| \boldsymbol{w} \|^{\boldsymbol{2}}$. By constructing a Lagrange function and solving a quadratic programming problem, $f(\boldsymbol{x})$ can be written in the following final form:

$$f(\boldsymbol{x}) = \sum_{i=1}^{n} \{(\alpha_i - \hat{\alpha}_i)K(\boldsymbol{x_i}, x) + b\} \tag{2}$$

where $K(\boldsymbol{x_i}, \boldsymbol{x})$ is a kernel function that replaces the product $\boldsymbol{\Phi}^T(\boldsymbol{x_i})\boldsymbol{\Phi(x)}$, and enables using low dimensional space data without knowing the transformation. The coefficients $\alpha_i, \hat{\alpha}_i$ are Lagrange multipliers, and b is the bias constant that is determined using Karush–Kuhn–Tucker (KKT) conditions [42], [43]. The radial basis function is typically used as the kernel for regression

$$K(\boldsymbol{x_i}, \boldsymbol{x}) = \exp\left(\frac{\|\boldsymbol{x_i} - x\|^{\boldsymbol{2}}}{2\sigma^2}\right). \tag{3}$$

For all training examples that $|f(\boldsymbol{x_i}) - y_i| < \varepsilon$, the Lagrange multipliers $\alpha_i\hat{\alpha}_i$ are equal to zero. Only for training data that $|f(\mathbf{x_i}) - y_i| \geq \varepsilon$, the Lagrange multipliers may be nonzero. The examples with nonzero coefficients are called *support vectors* and contribute in the regression function $f(\boldsymbol{x})$. Detailed descriptions of ν-SVR algorithm are provided in [44] and [45].

III. Methods

Ten able-bodied subjects (ages: 21–42, all right handed), and two individuals with transradial limb deficiency (LD) participated in this work. The first LD subject (male, age: 42) had a congenital absence with a long residual forearm [Fig. 1(a)]. The second LD subject (male, age: 62) had a traumatic amputation

TABLE I
WRIST AND FOREARM PRACTICAL CONTRACTIONS INCLUDED IN THE PROTOCOL FOR ABLE-BODIED SUBJECTS. FOR THE LD SUBJECTS, THE CONTRACTIONS INVOLVING ABDUCTION–ADDUCTION DOF WERE REMOVED

Index	Contraction
1	Flexion
2	Extension
3	Abduction
4	Adduction
5	Pronation
6	Supination
7	Simultaneous Flexion and Pronation
8	Simultaneous Flexion and Supination
9	Simultaneous Extension and Pronation
10	Simultaneous Extension and Supination
11	Simultaneous Abduction and Pronation
12	Simultaneous Abduction and Supination
13	Simultaneous Adduction and Pronation
14	Simultaneous Adduction and Supination

(since six years ago) with a medium length residual forearm and substantial scarring of the distal end [Fig. 1(b)]. The first LD subject had a brief experience with myoelectric control decades earlier, and the second LD subject was a regular user of a myoelectric prosthesis.

The experimental protocol was approved by the University of New Brunswick's Research Ethics Board. Three wrist DOFs including wrist flexion–extension, abduction–adduction, and pronation–supination were investigated. Pilot studies showed that amputees have difficulties in executing all three DOFs of wrist simultaneously, and therefore the abduction–adduction DOF was removed from the protocol to simplify the task. Eight bipolar wireless surface electrodes (Delsys Inc.) were attached around the circumference of the dominant (or affected, in the case of the LD subjects) forearm. The electrodes were placed proximally one third of the forearm length, measured from the olecranon of ulna. The EMG data were sampled at 1 KHz using a 16 bit A/D converter (NI PCIe-6363). The experiment was conducted in one session and included a training session and Fitts' law tests. Sufficient rest time was provided during the experiment to avoid fatigue. The experiment involved 14 practical contractions listed in Table I (eight contractions for LD subjects as the abduction–adduction DOF was removed).

The data acquisition and processing was conducted using MATLAB.

A. Training Protocol

A cursor capable of vertical and horizontal movement and rotation was displayed on a computer screen (Fig. 2). The subjects were prompted to elicit contractions according to cursor displacements. The horizontal, vertical, and orientation displacement of the cursor represented wrist flexion–extension, abduction–adduction, and pronation–supination, respectively. For the LD subjects, the cursor vertical displacement was zero as the abduction–adduction DOF was removed from the protocol. The contraction intensity in a given DOF was dictated by the cursor

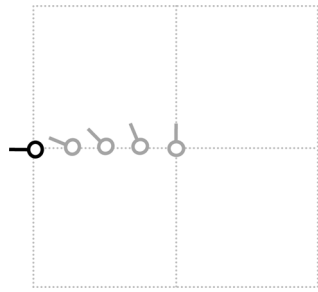

Fig. 2. Training protocol: the movement of the cursor (grey) from the neutral position towards the target (black), is shown. This movement corresponds to simultaneous flexion and pronation (when using right forearm).

displacement in the corresponding direction. The training protocol included 14 (eight in the case of LD subjects) trials associated with the contractions of Table I. A fixed 2-D target was displayed with location and orientation corresponding to the maximum deviation, as well as a picture of the prompted contraction.

Each dynamic movement was 7 s in duration and included 1 s of initial *no motion* while the cursor was at the screen center with vertical orientation (neutral position), 1.5 s of transition to the full range contraction (from Table I) during which the cursor was moving towards the target, 2 s of maintaining the full range contraction as the cursor was on the target, 1.5 s of returning to *no motion* while the cursor was moving towards the neutral position, followed by maintaining *no motion* for the remaining 1 s as the cursor was at the neutral position. Each trial included four repetitions of a movement. The subjects were instructed to employ a comfortable range of contraction intensity. During combined motions, the users were asked to increase/decrease the active DOFs simultaneously, as prompted by the cursor simultaneous movements in both directions. The EMG data and corresponding cursor displacements were recorded, concurrently.

B. Data Processing

The EMG data were filtered between 10–450 Hz using a third-order Butterworth bandpass filter. The time domain (TD) features including *mean absolute value*, *waveform length*, *zero crossings*, and *slope signs changes* were computed using a window length of 200 ms and an increment of 50 ms as in [21].

The cursor displacements in every DOF were scaled between $[-1, 1]$, where zero displacement in all DOFs (neutral position) corresponded to *no motion*, while a displacement of unity magnitude in a given DOF represented the maximum desired contraction. An ANN-based system and an SVM-based system were trained for EMG-based motion intent estimation. For the ANN-based scheme, a separate multilayer perceptron was used for each DOF as in [21]. The ANNs had a single hidden layer with five neurons, where the hidden and output layers had tan-sigmoid and linear activation functions, respectively. The training algorithm was Levenberg–Marquardt back-propagation. The SVM-based system used the ν-support vector regression (ν-SVR) algorithm (pilot studies showed the performance was approximately the same as that of the ϵ-SVR). A separate SVM was used for each DOF. The SVM configuration was determined using pilot data to achieve maximum offline estimation accuracy (R^2). The optimum configuration

was found to be the radial basis function as the kernel type, $\nu = 0.5$, and $\gamma = ((1)/(\text{number of features})) = ((1)/(32))$. The optimum value of *cost* parameter was found to be 0.2, because increasing the *cost* higher than 0.2, did not improve the R^2, but increased the training time. The SVM simulation was performed using the libsvm MATLAB package.[1] The functions *fitnet* and *svmtrain* were used to implement the ANN and SVM.

For a given DOF, the corresponding ANN/SVM was trained using the EMG TD features as the inputs and the cursor horizontal (for flexion–extension), vertical (for abduction–adduction), and orientation (for pronation–supination) displacement as the target.

The offline estimation accuracy was determined using a four-fold estimation cross-validation, where three out of four movement repetitions in every trial were included in the training set and the remaining repetition was used in the test set (75% training, 25% testing). The coefficient of determination (R^2) of (4) was employed to evaluate the offline estimation accuracy in each DOF

$$R_j^2 = 1 - \frac{\sum_{t=0}^{M} (\hat{f_j}(t) - f_j(t))^2}{\sum_{t=0}^{M} \left(f_j(t) - \overline{f_j(t)}\right)^2} \tag{4}$$

where $f_j(t)$ is the cursor displacement associated to the jth DOF (e.g., for abduction-adduction, the vertical displacement), $\widehat{f_j(t)}$ is the corresponding estimated output, $\overline{f_j(t)}$ is the temporal average of $f_j(t)$, M is the number of data samples, and R_j^2 is the coefficient of determination for the jth DOF. The estimated outputs were lowpass filtered with a cutoff frequency of 1 Hz to match the target bandwidth.

C. Fitts' Law Test

A 3-D (2-D in case of LD subjects) Fitts' law style real-time target acquisition test was performed to assess the usability of the ANN-based and SVM-based control schemes. The estimated motion intent in each DOF was mapped to the velocity in the corresponding direction of a control cursor with orientation. *Velocity control* was chosen as it is more relevant to prosthesis applications which are the focus of this work. During the test, a fixed 2-D target with orientation was presented on the screen and the users were prompted to reach the target as quickly as possible (for LD subjects, the target and cursor vertical displacements were zero).

Fitts' law test uses a single measure called *throughput* (*TP*) to evaluate the target acquisition performance. *Throughput* is measured in bits per second and is formulated as

$$TP = \frac{1}{N} \sum_{i=1}^{N} \frac{ID_i}{MT_i} \tag{5}$$

where N is the total number of conditions, i is a particular movement condition, *MT* is the time (in seconds) to acquire the target, and *ID* is the target index of difficulty (in bits) defined as

$$ID = \log_2 \left(1 + \frac{D}{W}\right) \tag{6}$$

[1]Available online: http://www.csie.ntu.edu.tw/~cjlin/libsvm

TABLE II
TARGET DISTANCES AND WIDTHS AND THE RESULTING INDEXES OF DIFFICULTY

Distance	*Width*	*ID*
1	0.10	3.46
1	0.15	2.94
1	0.25	2.32
0.5	0.10	2.59
0.5	0.15	2.12
0.5	0.25	1.59

where D and W are the target distance and width, respectively.

To successfully acquire a target, the 3-D (2-D in the case of LD subjects) Euclidean distance between the cursor and target had to be maintained lower than half the target width (W) for a *dwell time* of one second. If this distance was smaller than $W/2$, the cursor color changed as feedback. If the target was not achieved within 15 s, the task was timed out, and was regarded as a failure. Targets with combinations of three different widths and two different distances were used resulting in six indexes of difficulty as shown in Table II. Targets corresponding to the contractions of Table I were employed. For a combined DOF target with distance of D, the distance of each nonzero DOFs was $(D)/(\sqrt{2})$. Since small target widths were used, reaching a target required a small distance in each of the three DOFs between the cursor and target. Therefore, a high control performance in every DOF was required.

The average processing time for estimation of a single sample using an ANN and an SVM was 20 ms and 2 ms, respectively. This allowed a faster screen update rate during SVM-based control test. For the SVM control, the three SVMs required on average 6 ms. Considering the rendering and other data processing and a margin time (as the processing times are variable), the screen was updated every 40 ms. For the ANN control, the three ANNs required on average 60 ms. Including the rendering and other data processing and a margin time (a larger value was used as the ANN processing time variance was higher than that of the SVM), the screen was updated every 100 ms (for the LD subjects' test, the screen was updated every 80 ms for the ANN control, as two DOFs and consequently two ANNs were used).

To determine the effect of the estimation accuracy and processing speed separately, an additional SVM-based scheme was included. With this system, delay was added before each rendering so that the screen was updated with the same rate as the ANN-based system i.e., every 100 ms (80 ms for LD subjects). This system is referred to as the *SVM-delayed*.

Targets corresponding to the contractions of Table I with different indexes of difficulty of Table II were included, resulting in $14 \times 6 = 84$ (48, for LD subjects) targets for each control scheme. For every subject and control scheme, the order of targets was randomized, and divided into six trials of 14 targets. For each subject, a complete test involved $84 \times 3 = 252$ (144, for

TABLE III
ADDITIONAL PERFORMANCE METRICS INCLUDED FOR CONTROL ASSESSMENT

Metric	Description
Completion Rate	Describes the task success; the percentage of the acquired targets within the allowed 15 seconds time.
Path Efficiency	Describes the control quality; the mean of the ratio between the shortest 3-D distance to the target and the travelled 3-D distance.
Overshoot	Describes the target acquisition ability; the average number of times the target was reached and lost before completing the dwell time.

LD subjects) targets. To perform six trials, each trial was completed using the three control schemes (ANN, SVM, SVM-delayed) performed in random order, before proceeding to the next trial. This random order was different for each trial and for each subject. The users were blind with respect to the control scheme used in each test.

In addition to *throughput*, other performance metrics used in [35], [46] including the *completion rate, path efficiency*, and *overshoot* were computed as listed in Table III, to assess various aspects of the control quality.

The velocity gain of the control cursor relating the estimated output to the cursor speed was determined in a pilot study as 0.6 units per second. This value was chosen because among the gains with highest *throughput*, it resulted in the highest *path efficiency* and lowest *overshoot*.

In every DOF, for estimated outputs with magnitudes lower than predefined thresholds, the cursor speed in the corresponding DOF was set to zero. This was used to improve the control quality and to ensure the cursor stopped when the user performed *no motion*. The thresholds were determined based on offline estimates during *no motion* periods. The thresholds (*TH*) for the ANN- and SVM-based systems were found independently, and for every subject and DOF, as follows:

$$TH = \min\{0.2, (\mu_y + 3\sigma_y)\} \tag{7}$$

where μ_y and σ_y are the mean and standard deviation of the offline estimates absolute values of the corresponding DOF during *no motion*. The value of $(\mu_y + 3\sigma_y)$ was greater than 99% of the estimates during *no motion*. A maximum allowed threshold of 0.2 i.e., 20% of full range (determined empirically) was used to prevent excessive reduction of motion range. To avoid cursor speed discontinuity due to the use of threshold, the output range above the threshold in each DOF was mapped to the speed range [47], as follows:

$$\begin{aligned} &\text{if } |x| > TH |v| = \frac{|x| - TH}{1 - TH} \\ &\text{if } |x| < TH |v| = 0 \end{aligned} \tag{8}$$

where x is the estimated real-time output in a DOF, and $|v|$ is the cursor speed magnitude in the corresponding DOF. This method allowed the user to generate near zero speeds, despite their contraction intensity being above the threshold.

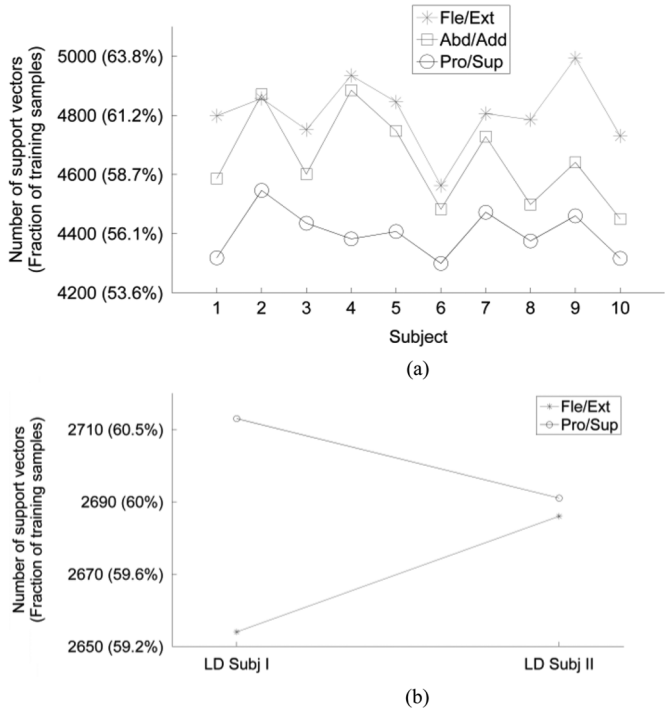

Fig. 3. Number of support vectors for each SVM is shown using the absolute value and fraction (%) of the training samples (the latter in brackets) for the (a) able-bodied subjects and (b) LD subjects.

D. Statistics

The offline estimation accuracies of the ANN- and SVM-based methods were compared using a one way repeated measures ANOVA test. The real-time control performance metrics of the ANN-, SVM-, and SVM-delayed schemes were compared using a one way repeated measures ANOVA test followed by a *Tukey-Kramer* post hoc test. The significance level was set to 0.05.

IV. RESULTS

A. Offline Results

The numbers of support vectors for the SVMs are shown for each subject in Fig. 3 using both the absolute value and fraction of the training samples (the latter in brackets). The offline cursor displacement estimation accuracies (R^2) averaged across able-bodied subjects and for each LD subject are depicted in Fig. 4 for the ANN and SVM. For able-bodied users, no significant difference was found between the offline R^2 of the ANN- and SVM-based systems in any DOF (the p values were 0.42, 0.96, and 0.47 for flexion–extension, abduction–adduction, and pronation–supination, respectively). For the LD subjects, the R^2 values of the SVM were similar to those of the ANN, except that for the first LD subject, the SVM outperformed the ANN in pronation–supination.

To determine the relative performance of the two estimators, their behavior was investigated more closely. Specifically, the estimation accuracy of each DOF during its *inactive* periods was examined. *Inactive* periods for a DOF are when the target displacement in that DOF is zero, but in other DOFs could be either

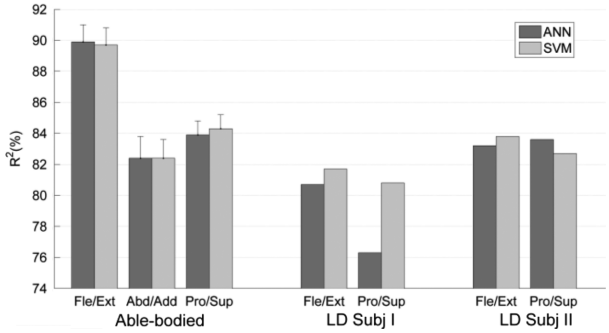

Fig. 4. Offline estimation accuracies R^2 (%) averaged across able-bodied subjects are shown using mean ± standard error. R^2 values (%) for each LD subject are demonstrated, separately.

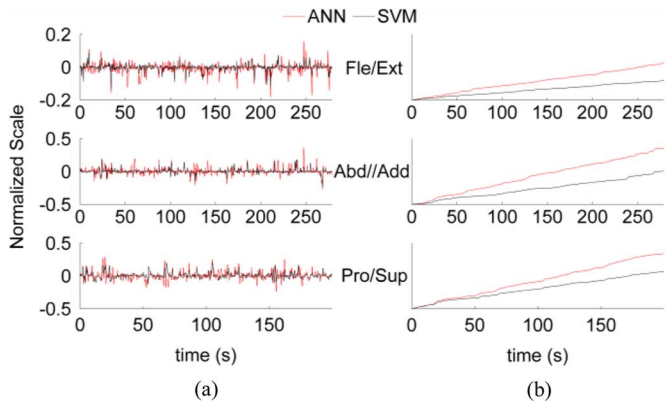

Fig. 5. (a) Estimated outputs during inactive periods using ANNs and SVMs for a representative subject, (b) the corresponding cumulative sums of the estimates absolute values during inactive periods.

zero or nonzero. This is different from *no motion* periods (which are a subset of *inactive* periods) that denote when all DOFs are zero.

The standard deviations of the offline estimation error (%) during *inactive* periods of each DOF averaged across able-bodied subjects are listed in Table IV, where the results for LD subject I and II are shown in brackets, respectively. The statistical analyses results are also included for able-bodied subjects. The results of both able-bodied and LD subjects demonstrate that the SVM outperformed the ANN during *inactive periods* for every DOF. The estimated outputs during inactive periods of each DOF are plotted for a representative subject in Fig. 5(a). The corresponding cumulative sums of the estimates absolute values are plotted in Fig. 5(b), which show that the estimation error of the ANN was higher than that of the SVM in every DOF.

For further investigation, the performance was assessed during different levels of contraction intensity, separately. For every DOF, the estimation error was computed for low, medium and high amplitudes during which the target cursor amplitude in the corresponding DOF was less than 20%, between 20% and 60%, and greater than 60% of the full range, respectively. The standard deviations of the corresponding offline estimation errors (%) averaged across able-bodied subjects are listed in Table V, where the results for LD subject I and II are shown

TABLE IV
STANDARD DEVIATIONS OF THE OFFLINE ESTIMATION ERROR (%) DURING INACTIVE PERIODS AVERAGED ACROSS ABLE-BODIED SUBJECTS ARE LISTED USING MEAN ± STANDARD ERROR. RESULTS FOR LD SUBJECT I AND II ARE SHOWN IN BRACKETS, RESPECTIVELY. STATISTICAL ANALYSES FOR ABLE-BODIED SUBJECTS ARE ALSO INCLUDED AND SIGNIFICANT COMPARISONS ARE MARKED WITH*

	ANN	*SVM*	*p-value*
Fle/Ext	6.1 ± 0.5 (15.5)(12.2)	4.1 ± 0.3 (12.0)(8.6)	<0.001*
Abd/Add	9.2 ± 0.5	6.6 ± 0.5	<0.001*
Pro/Sup	10.0 ± 0.3 (14.5)(7.7)	7.3 ± 0.2 (11.8)(5.8)	<0.001*

TABLE V
STANDARD DEVIATIONS OF THE OFFLINE ESTIMATION ERROR (%) AVERAGED ACROSS ABLE-BODIED SUBJECTS ARE SHOWN FOR LOW, MEDIUM, AND HIGH AMPLITUDES USING MEAN ± STANDARD ERROR. RESULTS FOR LD SUBJECT I AND II ARE SHOWN IN BRACKETS, RESPECTIVELY. STATISTICAL ANALYSES FOR ABLE-BODIED SUBJECTS ARE ALSO INCLUDED AND SIGNIFICANT COMPARISONS ARE MARKED WITH*

		ANN	*SVM*	*p-value*
Low amplitudes	*Fle/Ext*	6.7 ± 0.5 (15.5)(13.1)	5 ± 0.3 (12.4)(9.9)	<0.001*
	Abd/Add	9.7 ± 0.5	7.2 ± 0.4	<0.001*
	Pro/Sup	10.6 ± 0.3 (15.7)(9.6)	8.2 ± 0.2 (12.8)(7.3)	<0.001*
Medium amplitudes	*Fle/Ext*	21.1 ± 1.1 (26.2)(23.4)	22.1 ± 1.1 (26.6)(23.7)	0.28
	Abd/Add	25.9 ± 1.1	26.5 ± 1.0	0.16
	Pro/Sup	25.5 ± 0.6 (28.2)(22.5)	25.9 ± 0.8 (28.3)(23.3)	0.40
High amplitudes	*Fle/Ext*	17.4 ± 1.0 (22.7)(24.3)	20.5 ± 1.2 (24.4)(26.1)	<0.001*
	Abd/Add	23.4 ± 1.1	26.7 ± 1.3	0.001*
	Pro/Sup	22.6 ± 0.9 (26.4)(23.7)	24.7 ± 0.9 (24.4)(28.3)	0.009*

in brackets, respectively. The statistical analyses results for able-bodied subjects are also listed, which demonstrate that in every DOF, the SVM outperformed the ANN in low amplitudes, while the ANN outperformed the SVM in high amplitudes. No significant difference was found between the two estimators in medium amplitudes. For both LD subjects, the SVM outperformed the ANN in low amplitudes, while for medium amplitudes the results were similar between ANN and SVM. For high amplitudes, with LD subject I, the ANN outperformed the SVM in flexion–extension, but the SVM outperformed the ANN in pronation–supination. With LD subject II, the ANN outperformed the SVM during high amplitudes. Table VI lists the threshold values computed using (7) averaged across able-bodied subjects, where the threshold values for LD subject I and II are shown in brackets, respectively.

B. Fitts' Law Test Results

The real-time test results obeyed the Fitts' law since, as shown in Fig. 6, significant linear relationships $(R^2 > 0.95)$

TABLE VI
THRESHOLD VALUES FOR EACH CONTROL SCHEME AVERAGED ACROSS ABLE-BODIED SUBJECTS ARE LISTED USING MEAN ± STANDARD ERROR. RESULTS FOR LD SUBJECT I AND II ARE SHOWN IN BRACKETS, RESPECTIVELY. SCALES ARE NORMALIZED AS THE UNITY MAGNITUDE CORRESPONDS TO THE FULL RANGE CONTRACTION

	ANN	*SVM*
Fle/Ext	0.14 ± 0.01 (0.2)(0.2)	0.09 ± 0.01 (0.2)(0.2)
Abd/Add	0.18 ± 0.009	0.12 ± 0.02
Pro/Sup	0.16 ± 0.007 (0.2)(0.2)	0.12 ± 0.01 (0.2)(0.15)

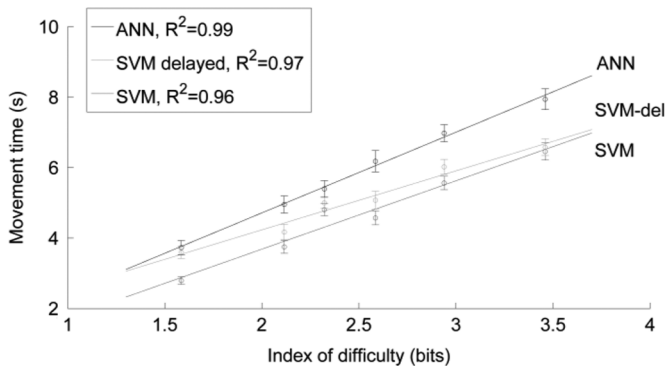

Fig. 6. Relationships between movement time and index of difficulty for each control scheme for able-bodied subjects.

were found between the movement times and indexes of difficulty in every control scheme. Fig. 7 depicts a 3-D representation (where cursor orientation is shown in the Z-direction for visualization purposes) of cursor path traces during the Fitts' law test for a representative subject for (a) ANN and (b) SVM-delayed systems (only the first 10 achieved targets are shown for clarity). The Fitts' law test results averaged across able-bodied and for each LD subject are shown in Fig. 8. The statistical analyses results for able-bodied subjects are shown in Table VII, and demonstrate that the SVM and SVM-delayed control schemes outperformed the ANN-based system in all four control performance metrics. Also, the throughput of the SVM system was higher than that of the SVM-delayed, but no significant difference was found between the SVM and SVM-delayed systems in other performance metrics.

For LD subject I, The SVM-delayed outperformed the ANN in *throughput* and *path efficiency*, but in *overshoot* and *completion rate* the results were similar between the ANN and SVMdelayed. Also, the *throughput* of the SVM was higher than that of the SVM-delayed, but the other metrics performances were similar between SVM and SVM-delayed.

For LD subject II, the SVM-delayed outperformed the ANN in *throughput*, while in other metrics the performances were similar between ANN and SVM-delayed. Also, no major difference was found between the results of the SVM and SVM-delayed.

To obtain a measure of performance with combined motions during the Fitts' law test, a metric β was defined as the ratio

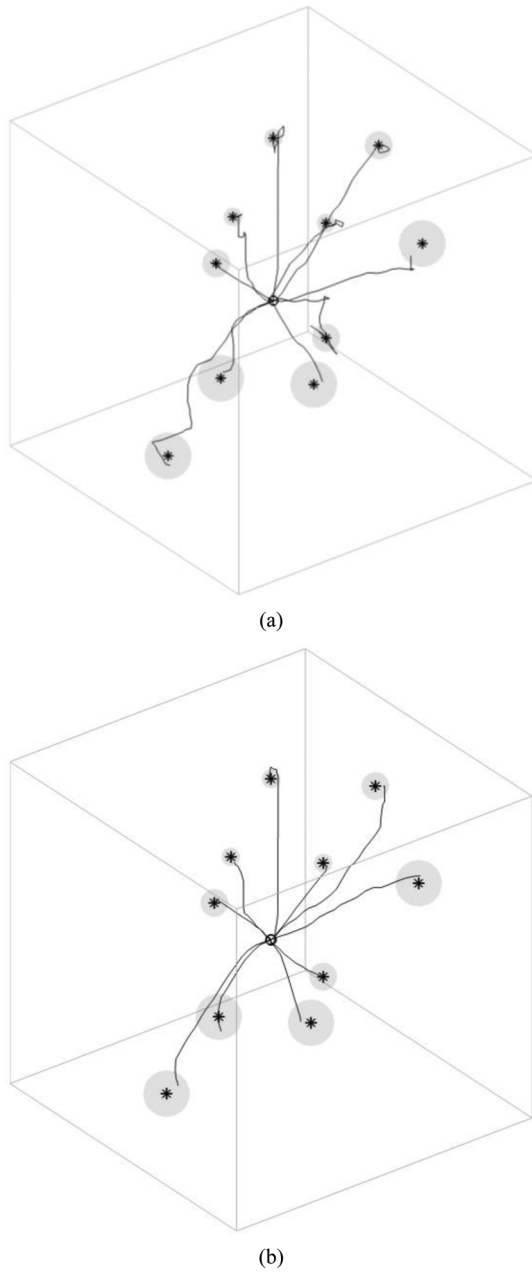

Fig. 7. A 3-D representation of path traces for a representative subject in the Fitts' law test; the first 10 acquired targets are shown for clarity for (a) ANN, (b) SVM-delayed control schemes.

between the number of times that multiple DOFs were greater than 40% of full range and number of times that only one DOF was larger than 40% of full range. Table VIII lists the β values averaged across able-bodied subjects computed separately for single and combined DOF targets, where the results for LD subject I and II are presented in brackets, respectively. The statistical comparisons between the two target types are included in Table VIII for able-bodied users, which demonstrate that the occurrence of combined motions during combined DOF targets was significantly higher than that during single DOF targets. Similarly, for LD subject I, the β values for combined DOF targets was considerably higher than those of single DOF targets. However, for LD subject II, the difference of β values between

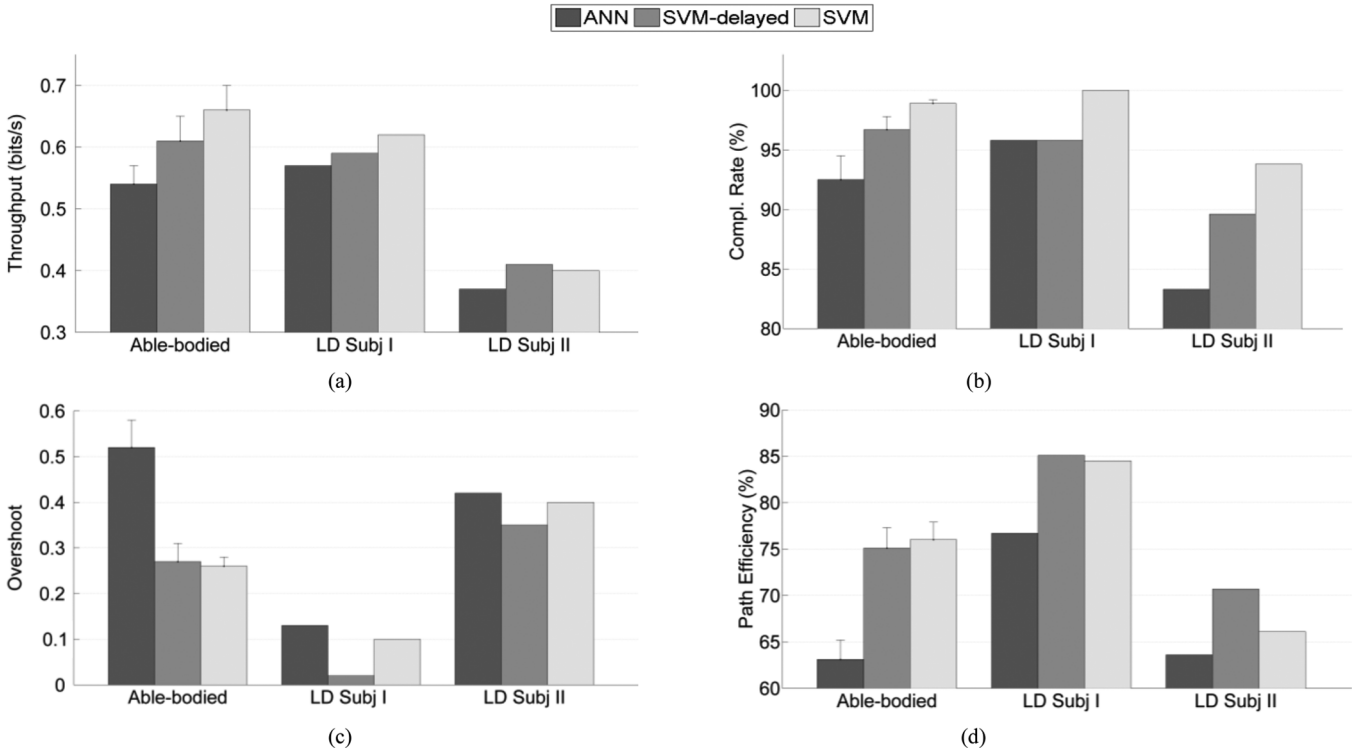

Fig. 8. Fitts' law test results averaged across able-bodied subjects are shown using mean ± standard error. Also, the results for each LD subject are demonstrated, separately. Plots show the results for (a) throughput (bits/s), (b) completion rate (%), (c) overshoot, and (d) path efficiency (%).

TABLE VII
STATISTICAL ANALYSES OF THE FITTS' LAW TEST RESULTS FOR ABLE-BODIED SUBJECTS (SIGNIFICANT COMPARISONS ARE MARKED WITH*)

	ANN vs SVM	*ANN vs SVM-delayed*	*SVM vs SVM-delayed*
Throughput	$p<0.001$*	$p<0.001$*	$p=0.002$*
Completion rate	$p=0.001$*	$p=0.03$*	$p>0.1$
Overshoot	$p<0.001$*	$p<0.001$*	$p>0.1$
Path Efficiency	$p<0.001$*	$p<0.001$*	$p>0.1$

TABLE VIII
THE β VALUES AVERAGED ACROSS ABLE-BODIED SUBJECTS ARE SHOWN USING MEAN ± STANDARD ERROR. RESULTS FOR LD SUBJECT I AND II ARE SHOWN IN BRACKETS, RESPECTIVELY. STATISTICAL COMPARISONS BETWEEN SINGLE AND COMBINED DOF TARGETS ARE ALSO INCLUDED FOR ABLE-BODIED SUBJECTS AND THE SIGNIFICANT COMPARISONS ARE MARKED WITH*

	Single DOF targets	*Combined DOFs targets*	*p-value*
ANN	0.24 ± 0.03 (0.07)(0.11)	0.62 ± 0.04 (0.45)(0.31)	<0.001*
SVM-delayed	0.08 ± 0.02 (0.03)(0.08)	0.69 ± 0.11 (0.49)(0.16)	<0.001*
SVM	0.11 ± 0.03 (0.01)(0.07)	0.73 ± 0.10 (0.50)(0.16)	<0.001*

single and combined DOF targets was not as large as that with able-bodied users and LD subject I.

The histograms of the cursor speeds in each DOF during the Fitts' law test, averaged across able-bodied subjects are plotted in Fig. 9 for the ANN system. Since other control schemes and LD subjects' results yielded more or less similar histograms, they are not shown here. The results show that the speed in every DOF was less than 10% of the full range during the majority of the target acquisition time.

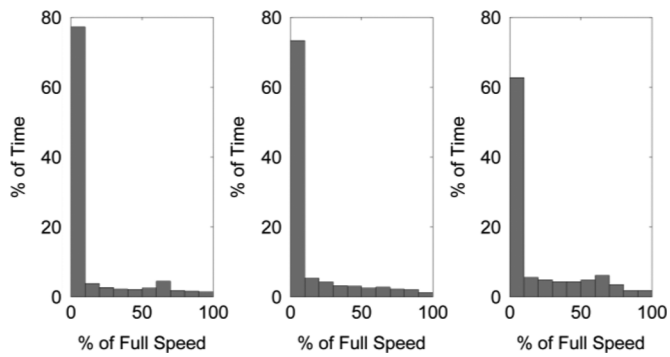

Fig. 9. Speed histograms for the ANN control scheme averaged across able-bodied subjects are shown. Plots from left to right correspond to flexion–extension, abduction–adduction, and pronation–supination.

V. DISCUSSION

A *visual target-based training* protocol was employed in this work, which can be potentially used for both unilateral and bilateral amputees. The control quality was evaluated using a *velocity*-based Fitts' law test. The *velocity control* is typically easier than *position control* for a user as the cursor movements are smoother (because the cursor displacements are integrals of the estimated intents, and therefore, estimates fluctuations do

not significantly affect the cursor movements). Moreover, maintaining the cursor on a target requires performing *no motion*, while with *position control* continuous contractions are needed. For these reasons, velocity control is commonly used in powered upper limb prostheses.

For low and high EMG amplitudes, the estimation accuracies of the ANNs were different from those of the SVMs (Table V). This was because the ANN and SVM have different modeling approaches, and also use different cost functions. For training an ANN, the cost function is the mean square error between the target and estimate. However, the SVM first uses a kernel trick to map the input data to a high dimensional feature space. For building the model, data with estimates close to the targets within a given threshold of ε are neglected, and only points outside the ε region (i.e., support vectors), contribute to the cost function. Also, the SVM seeks for the flattest function in the high dimensional feature space, to reduce the complexity of the model.

The SVM and SVM-delayed schemes outperformed the ANN system in all real-time control performance metrics with able-bodied subjects (Fig. 8 and Table VII). Qualitatively, all able-bodied users preferred the SVM and SVM-delayed control as they found fewer inadvertent cursor movements than those of the ANN scheme. This appears to be due to the relatively lower performance of the ANN during inactive and low amplitude periods of each DOF (Table V). Although the ANN outperformed the SVM in high amplitudes, it appears that the estimation accuracy in low amplitudes had more significant impact on the real-time control performance. This is likely because during the real-time control, low amplitudes were much more frequent than high amplitudes, as supported by the speed histograms demonstrating that the estimated outputs in every DOF were often low amplitude (Fig. 9). This is because in single DOF or two DOF contractions, other DOF(s) were inactive or low amplitude. Consider the case when a user performs pure flexion during control, poor estimation accuracy of inactive and low amplitude periods can result in inadvertent cursor movements in the DOFs other than flexion/extension. Consequently, instead of the exclusive cursor movement towards the left, unwanted cursor rotation may also occur due to poor estimation accuracy of the pronation–supination DOF, which can deteriorate all control performance metrics. Moreover, when the control cursor is close to a target, low amplitude contractions are required to generate low speeds, so that the target would not be missed. In this case, estimation error in low amplitude contractions can impede the target acquisition task, and adversely affect the performance metrics.

The speed thresholds were determined using *no motion* periods, to ensure the control cursor stopped when the user performed *no motion* (which was fulfilled successfully). If the thresholds are computed using *inactive* periods (where other DOFs can be zero or nonzero), the thresholds increase, and without limiting the values, this sometimes results in high thresholds for the ANNs (the average thresholds for abduction–adduction and pronation–supination would be 28%, and 30% of full range, respectively for able-bodied subjects). Therefore, when using the existing thresholds, some outliers may exceed the threshold, (due to poor estimation accuracy of especially the ANNs during inactive and low amplitude periods), and reduce the control quality. In this work, high thresholds, as those based on *inactive periods*, were not used because it removes much of the usable range of motion, and can adversely affect the control performance.

The LD subjects' Fitts' law test results in some cases outperformed those of the able-bodied subjects (Fig. 8). This was likely because the LD subjects' test was limited to two DOFs and therefore the target acquisition task was simpler than that of the able-bodied test requiring three DOFs control. The SVM-delayed outperformed the ANN in *path efficiency* and *throughput*, with LD subject I, and in *throughput* with LD subject II (Fig. 8). Similar to the able-bodied users, the higher performance of the SVM-based method can be attributed at least partially to more reliable characterization of inactive and low amplitude periods (Table V). Subjectively, LD subject I preferred the SVM and SVM-delayed control over the ANN control, while LD subject II did not find a major difference between the ANN and SVM-based systems but noted that the ANN felt slightly faster. In general, the difference between the results of the ANN and SVM-based control for the LD subjects was not as large as that with the able-bodied subjects. This is likely because the LD subjects' experiment was limited to two DOFs, and consequently the number of inactive DOFs was less than that of a three DOF experiment. As stated earlier, the advantage of the SVM over the ANN appears to be due to higher performance in inactive DOFs. With fewer DOFs under control (and therefore inactive DOFs during single DOF contractions), this advantage is reduced.

With able-bodied subjects, the throughput of the SVM scheme was higher than that of the SVM-delayed system (Fig. 8 and Table VII). This was due to the faster screen update rate of the SVM method that enhanced the efficacy of the user interaction with the system. The able-bodied subjects perceived the improved responsiveness of the SVM scheme and preferred it. With LD subject I, the *throughput* of the SVM was higher than that of the SVM-delayed, and with LD subject II, the *throughput* was similar between the SVM and SVM-delayed (Fig. 8). The LD subjects did not feel a major difference between the SVM and SVM-delayed systems. This was likely because the difference between the update rates of the SVM and SVM-delayed were less than that with able-bodied users.

All able-bodied subjects perceived and used simultaneous control of multiple DOFs. Based on Table VIII results, the use of combined motions with combined DOF targets was significantly higher than that with single DOF targets. This was expected as combined motions were not needed to reach single DOF targets, and shows that subjects performed combined motions to reach combined DOF targets (this is also supported by the high *path efficiency* values for all control schemes as shown in Fig. 8). It should be noted that if a combined DOF target was not acquired in the first try (e.g., due to overshoot), single DOF motions might be required to reach the target. Furthermore, for able-bodied users, the relatively high β values of the ANN control with single DOF targets (Table VIII) indicate some uses of combined motions. This is likely due to inadvertent cursor movements in inactive DOFs, so that the user had to perform combined motions to correct the unwanted movements.

The Fitts' law test results (Fig. 8) suggest a direct relationship between the control performance and length of the residual limb (this observation has also been reported by Jiang *et al.* [20]). This was expected, because longer residual muscles may enable more synergistic muscle activation which can improve the control ability. The subject with congenital absence (long stump) outperformed the traumatic amputee subject (medium length stump). However, it is not clear whether in general users with congenital or traumatic deficiency have higher myoelectric control ability, as other factors can impact performance, such as the type of amputation surgery (for traumatic amputees) and the absence or revision of motor pathways, which is highly variable within and between these populations.

Both LD subjects perceived simultaneous control. LD subject I comfortably performed combined motions during combined DOF targets. This is reflected in the high β values for combined DOF targets (Table VIII) and also high path efficiencies (Fig. 8). LD subject II's control performance was notably lower than that of LD subject I as supported by the Fitts' law test results (Fig. 8). LD subject II used combined motions for some combined DOF targets, but in many cases, he seemed to prefer performing sequential movements to achieve these targets (always first completing the desired rotation). This is reflected in the relatively low β values for combined DOF targets (Table VIII) and also low path efficiencies (Fig. 8). It is expected that LD subject II's simultaneous control would improve with practice and encouragement as he showed the ability to correctly generate combined DOF contractions when desired.

For the SVM, increasing either the *cost* parameter or ν leads to higher number of support vectors and consequently results in higher processing time for estimation. However, the increase of estimation time was not practically significant. For example, increasing the number of support vectors to 99% of the training samples would have increased the estimation time from 2 to 4 ms (for each SVM), which likely cannot be perceived by a user. For the ANN, it was found that dimensionality reduction was not useful to decrease the processing time for estimation. For instance, a considerable reduction of features from 32 to 8 did not change the ANN estimation time (20 ms for each ANN). ANNs may be significantly faster in embedded implementations.

A limitation of the approach used in this study is the increased duration of the training session with increasing the number of DOFs. Inclusion of combined motions is necessary for training, as pilot studies showed that removing combined motions from the training set reduced the offline estimation accuracy (R^2) significantly for both the SVM and ANN (the SVM slightly outperformed the ANN). The number of repetitions of contractions may be decreased to reduce the training session time. Also, using intramuscular EMG may improve performance of simultaneous control as indicated in [48].

VI. Conclusion

An SVM-based system was proposed for real time simultaneous myoelectric control of multiple DOFs. A Fitts' law test showed that the proposed scheme outperformed a baseline ANN-based method in all performance metrics for able-bodied subjects ($p < 0.05$). The SVM-based system outperformed the ANN control in *throughput* and *path efficiency* with the first LD subject, and in *throughput* with the second LD subject. The higher usability of the SVM-based method appears to be because of its higher estimation accuracy during inactive and low amplitude periods. The difference between the ANN- and SVM-based control schemes for the LD subjects was not as large as that for the able-bodied subjects. This is likely because the LD subjects' test was limited to two DOFs and consequently the number of inactive DOFs was less than that of a three DOF experiment. In addition to control performance improvement, the SVM-based method significantly lowered the numeric processing time for both training and real-time control.

References

[1] C. Cipriani, C. Antfolk, M. Controzzi, G. Lundborg, B. Rosen, M. C. Carrozza, and F. Sebelius, "Online myoelectric control of a dexterous hand prosthesis by transradial amputees," *IEEE Trans. Neural Syst. Rehabil. Eng.*, vol. 19, no. 3, pp. 260–270, Jun. 2011.

[2] P. K. Artemiadis and K. J. Kyriakopoulos, "An EMG-based robot control scheme robust to time-varying EMG signal features," *IEEE Trans. Inf. Technol. Biomed.*, vol. 14, no. 3, pp. 582–588, May 2010.

[3] J. M. Lambrecht, C. L. Pulliam, and R. F. Kirsch, "Virtual reality environment for simulating tasks with a myoelectric prosthesis: An assessment and training tool," *J. Prosthet. Orthot.*, vol. 23, no. 2, pp. 89–94, Apr. 2011.

[4] P. A. Parker, K. B. Englehart, and B. Hudgins, "Myoelectric signal processing for control of powered limb prostheses," *J. Electromyogr. Kinesiol.*, vol. 16, no. 6, pp. 541–548, 2006.

[5] D. S. Dorcas and R. N. Scott, "A three-state myoelectric controller," *Med. Biol. Eng.*, vol. 4, pp. 367–372, 1966.

[6] D. Childress, "A myoelectric three state controller using rate sensitivity," presented at the Int. Conf. Math. Biology and Ecology, Chicago, IL, 1969.

[7] T. W. Williams, "Practical methods for controlling powered upper-extremity prostheses," *Assist. Technol.*, vol. 2, no. 3, pp. 3–18, 1990.

[8] B. Hudgins, P. A. Parker, and R. N. Scott, "A new strategy for multifunction myoelectric control," *IEEE Trans. Biomed. Eng.*, vol. 40, no. 1, pp. 82–94, Jan. 1993.

[9] K. B. Englehart, B. Hudgins, P. A. Parker, and M. Stevenson, "Classification of the myoelectric signal using time-frequency based representations," *Med. Eng. Phys.*, vol. 21, no. 6–7, pp. 431–438, Jul.–Sep. 1999.

[10] Y. Huang, K. B. Englehart, B. Hudgins, and A. D. C. Chan, "Gaussian mixture model based classification scheme for myoelectric control of powered upper limb prostheses," *IEEE Trans. Biomed. Eng.*, vol. 52, no. 11, pp. 1801–1811, Nov. 2005.

[11] M. F. Lucas, A. Gaufriau, S. Pascual, C. Doncarli, and D. Farina, "Multichannel surface EMG classification using support vector machines and signal-based wavelet optimization," *Biomed. Signal Process. Control*, vol. 3, no. 2, pp. 169–174, Apr. 2008.

[12] L. Hargrove, E. Scheme, K. Englehart, and B. Hudgins, "Multiple binary classifications via linear discriminant analysis for improved controllability of a powered prosthesis," *IEEE Trans. Neural Syst. Rehabil. Eng.*, vol. 18, no. 1, pp. 49–57, Feb. 2010.

[13] E. Scheme and K. Englehart, "Training strategies for mitigating the effect of proportional control on classification in pattern recognition-based myoelectric control," *J. Prosthet. Orthot.*, vol. 25, no. 2, pp. 76–83, Apr. 2013.

[14] A. J. Young, L. H. Smith, E. J. Rouse, and L. J. Hargrove, "A new hierarchical approach for simultaneous control of multi-joint powered prostheses," in *IEEE RAS EMBS Int. Conf. BioRob.*, 2012, pp. 514–520.

[15] E. Kamavuako, J. Rosenvang, R. Horup, W. Jensen, D. Farina, and K. Englehart, "Surface versus untargeted intramuscular EMG based classification of simultaneous and dynamically changing movements," *IEEE Trans. Neural Syst. Rehabil. Eng.*, vol. 21, no. 6, pp. 992–998, Nov. 2013.

[16] J. L. Nielsen, S. Holmgaard, N. Jiang, K. B. Englehart, D. Farina, and P. A. Parker, "Simultaneous and proportional force estimation for multifunction myoelectric prostheses using mirrored bilateral training," *IEEE Trans. Biomed. Eng.*, vol. 58, no. 3, Mar. 2011.

[17] E. N. Kamavuako, D. Farina, K. Yoshida, and W. Jensen, "Estimation of grasping force from features of intramuscular EMG signals with mirrored bilateral training," *Ann. Biomed. Eng.*, vol. 40, no. 3, pp. 648–656, Mar. 2012.
[18] F. Sebelius, L. Eriksson, C. Balkenius, and T. Laurell, "Myoelectric control of a computer animated hand: A new concept based on the combined use of a tree-structured artificial neural network and a data glove," *J. Med. Eng. Tech.*, vol. 30, no. 1, pp. 2–10, Jan.–Feb 2006.
[19] S. Muceli and D. Farina, "Simultaneous and proportional estimation of hand kinematics from EMG during mirrored movements at multiple degrees of freedom," *IEEE Trans. Neural Syst. Rehabil. Eng.*, vol. 20, no. 3, pp. 371–378, May 2012.
[20] N. Jiang, J. L. Vest-Nielsen, S. Muceli, and D. Farina, "EMG-based simultaneous and proportional estimation of wrist/hand unconstraineds in uni-lateral trans-radial amputees," *J. Neuro. Eng. Rehabil.*, vol. 9, p. Epub, June 2012.
[21] A. Ameri, E. Scheme, E. Kamavuako, K. Englehart, and P. Parker, "Real time, simultaneous myoelectric control using force and position based training paradigms," *IEEE Trans. Biomed. Eng.*, vol. 61, no. 2, pp. 279–287, Feb. 2014.
[22] E. N. Kamavuako, J. C. Rosenvang, M. F. Bøg, A. Smidstrup, E. Erkocevic, M. J. Niemeier, W. Jensen, and D. Farina, "Influence of the feature space on the estimation of hand grasping force from intramuscular EMG," *Biomed. Signal Process. Control*, vol. 8, no. 1, pp. 1–5, Jan. 2013.
[23] J. M. Hahne, F. Biebmann, N. Jiang, H. Rehbaum, D. Farina, F. C. Meinecke, K. R. Muller, and L. C. Parra, "Linear and nonlinear regression techniques for simultaneous and proportional myoelectric control," *IEEE Trans. Neural Syst. Rehabil. Eng.*, vol. 22, no. 2, pp. 269–279, Mar. 2014.
[24] C. Castellini, E. Gruppioni, A. Davalli, and G. Sandini, "Fine detection of grasp force and posture by amputees via surface electromyography," *J. Physiol.-Paris*, vol. 103, pp. 255–262, Sep.–Dec. 2009.
[25] N. Jiang, H. Rehbaum, I. Vujaklija, B. Graimann, and D. Farina, "Intuitive, online, simultaneous and proportional myoelectric control over two degrees of freedom in upper limb amputees," *IEEE Trans. Neural Syst. Rehabil. Eng.*, vol. 22, no. 3, pp. 501–510, May 2014.
[26] S. Muceli, N. Jiang, and D. Farina, "Extracting signals robust to electrode number and shift for online simultaneous and proportional myoelectric control by factorization algorithms," *IEEE Trans. Neural Syst. Rehabil. Eng.*, vol. 22, no. 3, pp. 501–510, May 2014.
[27] C. Choi and J. Kim, "Synergy matrices to estimate fluid wrist movements by surface electromyography," *J. Med. Eng. Phys.*, vol. 33, no. 8, pp. 916–923, 2011.
[28] C. Castellini and P. Van der Smagt, "Surface EMG in advanced hand prosthetics," *Biol. Cybern.*, vol. 100, pp. 35–47, 2009.
[29] D. Yang, D. J. Zhao, Y. Gu, L. Jiang, and H. Liu, "EMG pattern recognition and grasping force estimation: Improvement to the myocontrol of multi-DOF prosthetic hands," in *Proc. IEEE/RSJ Int. Conf. Intell. Robots Syst.*, 2009, pp. 516–521.
[30] T. Tommasi, F. Orabona, C. Castellini, and B. Caputo, "Improving control of dexterous hand prostheses using adaptive learning," *IEEE Trans. Robotics*, vol. 29, no. 1, pp. 207–219, Feb. 2013.
[31] A. Ziai and M. Carlo, "Comparison of regression models for estimation of isometric wrist joint torques using surface electromyography," *J. Neuroeng. Rehabil.*, vol. 8, no. 1, 2011.
[32] P. Fitts, "The information capacity of the human motor system in controlling the amplitude of movement," *J. Exp. Psychol.*, vol. 47, no. 6, pp. 381–391, Jun. 1954.
[33] C. Shannon, "Mathematical theory of communication," *Bell Syst. Tech. J.*, vol. 27, pp. 623–656, 1948.
[34] J. Park, W. Bei, H. Kim, and S. Park, "EMG—Force correlation considering Fitts' Law," in *IEEE Int. Conf. Multisensor Fusion Integrat. Intell. Syst.*, Seoul, Korea, Aug. 2008, pp. 644–649.
[35] M. Williams and R. Kirsch, "Evaluation of head orientation and neck muscle EMG signals as command inputs to a human-computer interface for individuals with high tetraplegia," *IEEE Trans. Neural. Syst. Rehabil. Eng.*, vol. 16, no. 5, pp. 485–496, Oct. 2008.
[36] C. Choi, S. Micera, J. Carpaneto, and J. Kim, "Development and quantitative performance evaluation of a noninvasive EMG computer interface," *IEEE Trans. Biomed. Eng.*, vol. 56, no. 1, pp. 188–191, Jan. 2009.
[37] E. Scheme and K. Englehart, "Validation of a selective ensemble-based classification scheme for myoelectric control using a three dimensional Fitts' Law test," *IEEE Trans. Neural Syst. Rehabil. Eng.*, vol. 21, no. 4, pp. 616–623, Jul. 2013.
[38] E. Kamavuako, E. Scheme, and K. Englehart, "Combined surface and intramuscular EMG for improved real-time myoelectric control performance," *Biomed. Signal Process. Control*, vol. 10, pp. 102–107, 2014.
[39] C. Cortes and V. Vapnik, "Support-vector networks," *Mach. Learn.*, vol. 20, no. 3, pp. 273–297, 1995.
[40] B. Boser, I. Guyon, and V. Vapnik, "A training algorithm for optimal margin classifiers," in *Proc. 5th Annu. Workshop Computat. Learn. Theory*, Pittsburgh, PA, 1992, pp. 144–152.
[41] B. Scholkopf, P. Bartlett, A. Smola, and R. Williamson, "Shrinking the tube: A new support vector regression algorithm," in *Adv. Neural Inf. Process. Syst.*, 1999, pp. 330–336.
[42] W. Karush, "Minima of functions of several variables wiith inequalities as side constraints," M.S. thesis, Dept. Math., Univ. Chicago, Chicago, IL, 1939.
[43] H. Kuhn and A. Tucker, "Nonlinear programming," in *Proc. 2nd Berkeley Symp. Math. Stat. Probabilist.*, Berkeley, CA, 1951, pp. 481–492.
[44] C. Chang and C. Lin, "Training v-support vector regression: Theory and algorithms," *Neural Computat.*, vol. 14, no. 8, pp. 1959–1977, 2002.
[45] P. Chen, C. Lin, and B. Schölkopf, "A tutorial on v-support vector machines," *Appl. Stochastic Models Business Indust.*, vol. 21, no. 2, pp. 111–136, 2005.
[46] A. Simon, L. Hargrove, B. Lock, and T. Kuiken, "Target achievement control test: Evaluating real-time myoelectric pattern-recognition control of multifunctional upper-limb prostheses," *J. Rehabil. Res. Develop.*, vol. 48, no. 6, pp. 619–628, 2011.
[47] E. Scheme, B. Lock, L. Hargrove, W. Hill, U. Kuraganti, and K. Englehart, "Motion normalized proportional control for improved pattern recognition based myoelectric control," *IEEE Trans. Neural Syst. Rehabil*, vol. 22, no. 1, pp. 149–157, Jan. 2014.
[48] L. Smith and L. Hargrove, "Comparison of surface and intramuscular EMG pattern recognition for simultaneous wrist/hand motion classification," in *Proc. IEEE Conf. EMBS*, 2013, pp. 4223–4226.

Ali Ameri (S'10) received the B.Sc. degree from Sharif University of Technology, Tehran, Iran, and the M.Sc. degree in electrical engineering from Shahid Beheshti University, Tehran, Iran, in 2004 and 2007, respectively. He is currently a Ph.D. degree candidate in the Department of Electrical and Computer Engineering at the University of New Brunswick, Fredericton, NB, Canada.

His research interests include statistical signal processing, myoelectric control of powered prostheses, machine learning, and speech processing.

Ernest N. Kamavuako (M'11) received the M.S. and Ph.D. degrees in biomedical engineering from Aalborg University, Aalborg, Denmark, in 2006 and 2010.

Since 2014, he has been an Associate Professor in the Department of Health Science and Technology, Aalborg University, Denmark. From 2007 to 2008, he was a Research Scholar in the Biomedical Department, Indiana University–Purdue University Indianapolis, Indianapolis, IN, USA. From 2012 to 2013, he was a Visiting Postdoctoral Fellow at the Institute of Biomedical Engineering, University of New Brunswick, Fredericton, NB, Canada. His current research interests include the use of invasive recordings in the control of upper limb prostheses, muscle recovery functions following electrical stimulation, signal processing and the application of near-infrared spectroscopy for brain–computer interface and speech processing.

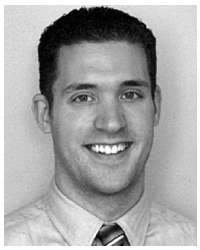

Erik J. Scheme (S'09–M'13) received the B.Sc., M.Sc., and Ph.D. degrees in electrical engineering from the University of New Brunswick (UNB), Fredericton, NB, Canada, in 2003, 2005, and 2013. respectively.

He is currently a Research Associate and New Brunswick Innovation Foundation Chair in Medical Devices and Technologies at the Institute of Biomedical Engineering at the University of New Brunswick (UNB), Fredericton, NB, Canada. His research interests include biological signal processing, pattern recognition, human–computer interfaces, and the clinical and commercial deployment of research.

Dr. Scheme is a Registered Professional Engineer.

Kevin B. Englehart (S'86–M'99–SM'03) received the B.Sc. degree in electrical engineering and the M.Sc. and Ph.D. degrees from the University of New Brunswick, Fredericton, NB, Canada, in 1989, 1992, and 1998, respectively.

He is the Director of the Institute of Biomedical Engineering at the University of New Brunswick, Fredericton, NB, Canada. His research interests include neuromuscular modeling and biological signal processing using adaptive systems, pattern recognition, and time-frequency analysis.

Dr. Englehart is a Registered Professional Engineer, and a Fellow of the Canadian Academy of Engineering. He is a member of the International Society of Electrophysiology and Kinesiology, and the Canadian Medical and Biological Engineering Society.

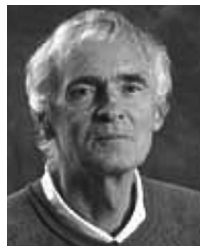

Philip A. Parker (S'70–M'73–SM'86–LSM'08) received the B.Sc. degree in electrical engineering and the Ph.D. degree from the University of New Brunswick, Fredericton, NB, Canada, in 1964 and 1975, respectively, and the M.Sc. degree from the University of St. Andrews, St. Andrews, U.K., in 1966.

In 1966, he joined the National Research Council of Canada as a Communications Officer. He is currently a Policy Board Member of the Institute of Biomedical Engineering, University of New Brunswick (UNB), Fredericton, NB, Canada, which he joined in 1967 as a Research Associate. In 1976, he was appointed to the Department of Electrical Engineering, UNB, where he is currently a Professor Emeritus. His current research interests include the area of biological signal processing with applications to powered limb prosthesis control, evoked response detection/estimation, conduction velocity distribution estimation, and diagnostic tools.